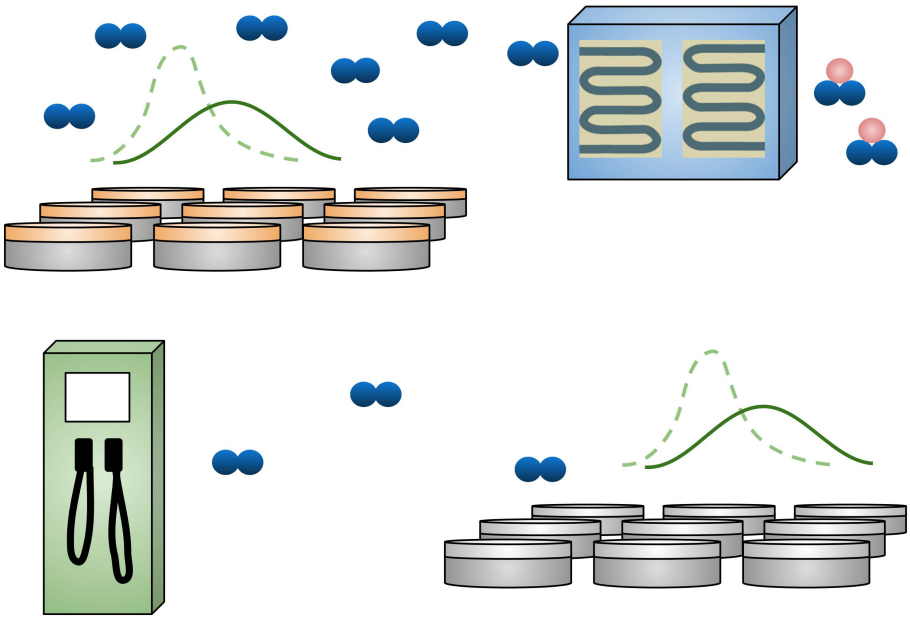

Nanoparticle based sensing for both high and low hydrogen concentration applications

Master's thesis in Physics

NOREA BJERDE

DEPARTMENT OF PHYSICS

CHALMERS UNIVERSITY OF TECHNOLOGY
Gothenburg, Sweden 2021
www.chalmers.se

Master's thesis 2021

Nanoparticle based sensing for both high and low hydrogen concentration applications

NOREA BJERDE

CHALMERS
UNIVERSITY OF TECHNOLOGY

Department of Physics
Division of Chemical Physics
Chalmers University of Technology
Gothenburg, Sweden 2021

Nanoparticle based sensing for both high and low hydrogen concentration applications
NOREA BJERDE

Supervisors: David Tomecek
Olof Andersson, Insplorion
Examiner: Christoph Langhammer, Department of Physics

Master's Thesis 2021
Department of Physics
Division of Chemical Physics
Chalmers University of Technology
SE-412 96 Gothenburg
Telephone +46 31 772 1000

Cover: Illustration of nanoplasmonic hydrogen sensing for fuel cell applications with PdCu alloy and safety applications with PdAg alloy.

Typeset in LaTeX
Printed by Chalmers Reproservice
Gothenburg, Sweden 2021

Nanoparticle based sensing for both high and low hydrogen concentration applications

NOREA BJERDE
Department of Physics
Chalmers University of Technology

Abstract

The hydrogen economy is the vision of a sustainable society where hydrogen is used as fuel for vehicles, heat generation and energy storage, with water as the only byproduct. To realize this vision, issues such as fuel cell efficiency and safety must be handled. Therefore, hydrogen sensors both for leak detection and fuel cell monitoring are needed. Palladium is known to have high selectivity in room temperature towards hydrogen gas, and it is therefore (especially in alloys) a promising candidate for this application. This study presents an investigation of several Pd alloy nanoplasmonic hydrogen sensors. Nickel and copper are metals of comparatively small lattice constants which increase the high concentration sensitivity of pure Pd. Silver has a comparatively large lattice constant and an ability to remove the effect of hysteresis which is also firmly connected with pure Pd. The Pd alloys of composition $Pd_{80}Ag_{20}$ and $Pd_{70}Ag_{30}$ both showed relatively large sensitivities in the 0.5-5 % region but a high limit of detection of 0.20 % for $Pd_{80}Ag_{20}$ and 0.38 % for $Pd_{70}Ag_{30}$. The kinetics of the alloys were slow with 138 s to 90 % response for $Pd_{80}Ag_{20}$ at 0.9 % H_2 versus 270 s for $Pd_{70}Ag_{30}$. The alloy compositions $Pd_{85}Ni_{15}$ and $Pd_{70}Cu_{30}$ resulted in sensors with linear response in the 5-95 % H_2 region with sensitivities 0.026 nm/% and 0.035 nm/% respectively. They had a limit of detection estimated to 0.71 % and 0.41 % and a precision of 2.8 % and 1.7 %. The linear response in the high concentration region indicates that both PdNi and PdCu are well suited for fuel cell hydrogen sensing.

Keywords: nanoplasmonic sensing, hydrogen sensor, palladium, nickel, copper, silver, alloy, hydrogen

Acknowledgements

I would like to thank everyone who has been helpful and made this work possible. I would like to thank my examiner Christoph Langhammer for introducing me to the subject of nanoplasmonic sensing and providing support along the way. Thanks also to Olof Andersson and Insplorion for giving me an opportunity to do my master's thesis in this field. I am very grateful for my brilliant supervisor David Tomecek who has been so generous with his time and taught me a lot about nanoplasmonic hydrogen sensing. Thank you for being patient with my questions, for conducting the nanofabrications and for helping me with all the test set-ups. I would like to thank Irem, Martin and the whole team at Insplorion for helping me to connect the subject to the application. Thank you for interesting meetings, discussion and guidance. Finally, I would like to thank Miriam for our discussions during this thesis work and for a great time together at Chalmers. It would not have been the same without you.

Norea Bjerde, Gothenburg, June 2021

Contents

List of Figures

List of Abbreviations

Ag Silver
Ar Argon
Au Gold
Bi Bismuth
CO Carbon monoxide
Cu Copper
FCC Face centered cubic
H Hydrogen
HCL Hole-mask colloidal lithography
IPA Isopropanol
LSPR Localized surface plasmon resonance
Mg Magnesium
Ni Nickel
O_2 Oxygen gas
Pd Palladium
PDDA Poly(diallyldimethylammonium chloride)
PID Proportional Integral Derivative
PMMA Poly(methyl methacrylate)
PS Polystyrene
Pt Platinum
PVD Physical vapor deposition

1

Introduction

1.1 Background

Since the beginning of the industrial revolution in the middle of the 18th century, fossil fuels have been used to power the society. With the burning of fossil fuels such as gas and oil comes the devastating consequence of large amounts of carbon dioxide released into the atmosphere, which enhances the natural greenhouse effect of the planet and causes higher temperatures. To meat the demand of our constantly increasing electrification without causing further global warming, sustainable and renewable energy solutions have to be developed.

One promising alternative is the so-called hydrogen economy illustrated in figure 1.1. The hydrogen economy is the vision of a sustainable society where hydrogen is used as fuel for vehicles, heat generation and energy storage, with water as the only byproduct. In this solution, hydrogen is produced by water electrolysis using renewable energy sources and then stored as the energy carrier. When needed, hydrogen is recombined with O_2 in a fuel cell to form water again and thereby generates electricity. [1]

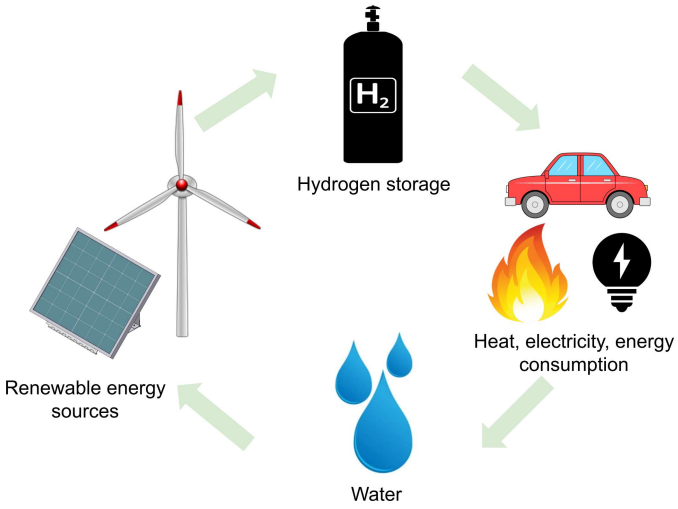

Figure 1.1: The hydrogen economy: hydrogen produced by splitting water using renewable energy sources is used as the energy carrier. The hydrogen is stored and later recombined with O_2 in a fuel cell, generating electricity.

To realize the vision of the hydrogen economy, challenges such as hydrogen

storage, transportation, fuel cell efficiency and safety must be handled [1]. The safety issue is critical if hydrogen is to function as an energy carrier as it is a highly reactive gas with a wide flammability range of 4-75 vol.%. Hydrogen is also transparent, odorless and very volatile. For this reason, there is a need for sensors that can detect low concentrations of hydrogen. The U.S. Department of Energy has put up target specifications for such hydrogen sensors including a measurement range of 0.01-10 % hydrogen concentration, response time less than 1 s and an accuracy of 5 %. Also for fuel cell development, there is a need for sensitive and safe hydrogen sensors for monitoring and controlling applications. For this cause, the sensor should have a measurement range of 50-100 % hydrogen in an inert atmosphere [2].

A relatively new and promising hydrogen sensor technology based on the phenomena of localized surface plasmon resonances (LSPR) in Pd nanoparticles was first presented in 2007 by Langhammer et al. [3]. LSPR is a term for the resonant oscillations of the conduction band electrons when the nanoparticle is illuminated with light with a wavelength longer or similar to the nanoparticle size. If Pd nanoparticles are exposed to hydrogen, a hydride is formed which causes lattice strain and a change in the permittivity. This in turn affects the LSPR wavelength and in this way, the wavelength can be used to monitor hydrogen concentration. Optical hydrogen sensors based on LSPR are safer than traditional electrical sensors in that regard that they do not generate sparks. Moreover, they provide remote readout, high sensitivity and and a compact size. [4]

However, there are some challenges with the Pd nanoparticle based hydrogen sensors. The Pd hydride formation is affected by the phenomena of hysteresis, which makes the sensor response nonspecific [4]. In addition, the LSPR wavelength has a logarithmic dependence on the hydrogen concentration. At high hydrogen concentrations, the response changes very slowly with the hydrogen concentration, meaning that the sensor has low sensitivity. For this reason, pure Pd is not well suited for fuel cell sensing applications. One suggested solution to these issues is to use alloys of Pd as nanoparticle materials. This has previously been done with e.g. PdAu, PdCu and PdPt [4, 5, 6]. PdAu has proven to mitigate the hysteresis of the sensor response and increase the sensitivity for low concentrations. Other alloys such as PdNi, PdAg and PdMg has been tested for thin film hydrogen sensing [7, 8, 9]. The PdNi alloy showed beneficial properties for high concentration sensing with high stability and large sensitivity, but the LSPR based sensing performance is yet unknown.

To look more into the sensor properties of different nanoparticle Pd alloys and find the optimal alloy for safety applications as well as fuel cell applications, further investigation is needed. In this study, a literature search for a optimal nanoparticle composition for safety as well as fuel cell applications is made. The suggested nanoparticle systems are then fabricated and evaluated on their sensitivity within the desired range, limit of detection and sensor kinetics.

1.2 Aim

The aim of the study is to suggest and evaluate nanoparticle systems optimal for hydrogen sensing in safety as well as fuel cell applications.

1.3 Delimitations

Due to the time limitation of the master's thesis, some delimitations are made. The study does not aim to include an evaluation of all relevant sensor properties such as tolerance towards humidity, poisoning and temperature changes. It neither includes details about the scaling process towards a final product. The main focus of the study is to perform a literature study on nanoparticle compositions as well as an experimental study of the nanoparticle based sensors which will pave the road to the systems that will function in desired applications.

1.4 Objectives

The following objectives are set up in order to reach the goal of suggesting and evaluating nanoparticle systems for hydrogen sensing:

1. Perform a literature study with the aim to suggest suitable nanoparticle systems for
   (a) detecting low concentrations of hydrogen at 1 bar in air for safety applications.
   (b) measuring high partial pressures of hydrogen in an inert atmosphere for fuel cell applications.
2. For the suggested nanoparticle systems, measure and calculate hydrogen sensor characteristics such as
   (a) pressure composition isotherm
   (b) detection limit
   (c) working range
   (d) response time
3. Analyze the results and evaluate the suggested nanoparticle systems on their high and low hydrogen concentration sensing performance.

2

Theory

2.1 Pd hydride formation

Pd has the ability to absorb large amounts of hydrogen in room temperature, and it is thereofore a suitable material for hydrogen storage but also sensing applications. The process of Pd hydride formation is presented in equation and figure 2.1. When hydrogen molecules approach a Pd surface they interact by Van der Waals forces with the Pd atoms. At the surface, the molecules are adsorbed and then dissociated into hydrogen atoms. After that, the atoms diffuse into subsurface interstitial sites before they go into bulk interstitial sites and form the Pd hydride, PdH_x, where x is the ratio of hydrogen to Pd. [10]

$$\mathrm{Pd} + \frac{x}{2}\mathrm{H_2} \longleftrightarrow \mathrm{PdH}_x \tag{2.1}$$

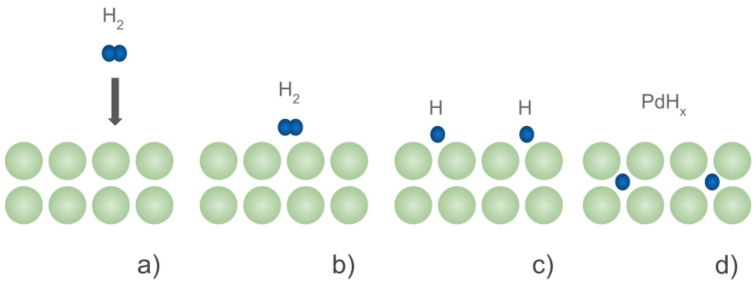

Figure 2.1: Pd hydride formation (adapted from [10]). a) Hydrogen molecules approaching the Pd surface. b) Physisorption where the hydrogen molecules are adsorbed on the surface. c) Chemisorption where hydrogen molecules dissociate into hydrogen atoms. d) Diffusion into subsurface and bulk interstitial sites.

The hydrogen absorption can be divided into three different stages or phases. A phase diagram for PdH_x together with a sketch of the α, β and $\alpha + \beta$ phase is presented in figure 2.2. At low hydrogen pressures, the atoms are sparsely distributed in the Pd lattice in a solid solution called the α phase. Here the hydrogen partial pressure, P_{H_2}, and the hydrogen concentration in the Pd, c_H, correlates to each other as Sieverts law, $\sqrt{P_{H_2}} = c_H K_S$, where K_S is the Sieverts constant. [10] As the concentration increases, areas of so-called β phase are formed where hydrogen atoms are distributed at neighbouring interstitial sites. This is called the coexisting $\alpha + \beta$ phase, and here the H/Pd ratio increases while the pressure remain constant,

which can be seen as a plateau in the phase diagram. The final β phase is when the Pd is fully hydrided. The maximum hydrogen solubilities in room temperature are 0.017 and 0.6 H/Pd for the α and β phase respectively [11]. The width of the phase transition plateau region decreases with increasing temperature. At the same time, the plateau region moves to higher pressures. Above a critical temperature, T_c, the plateau region completely vanishes and a continuous solid solution of Pd is obtained. For bulk Pd, T_c is about 290 °C. [12]

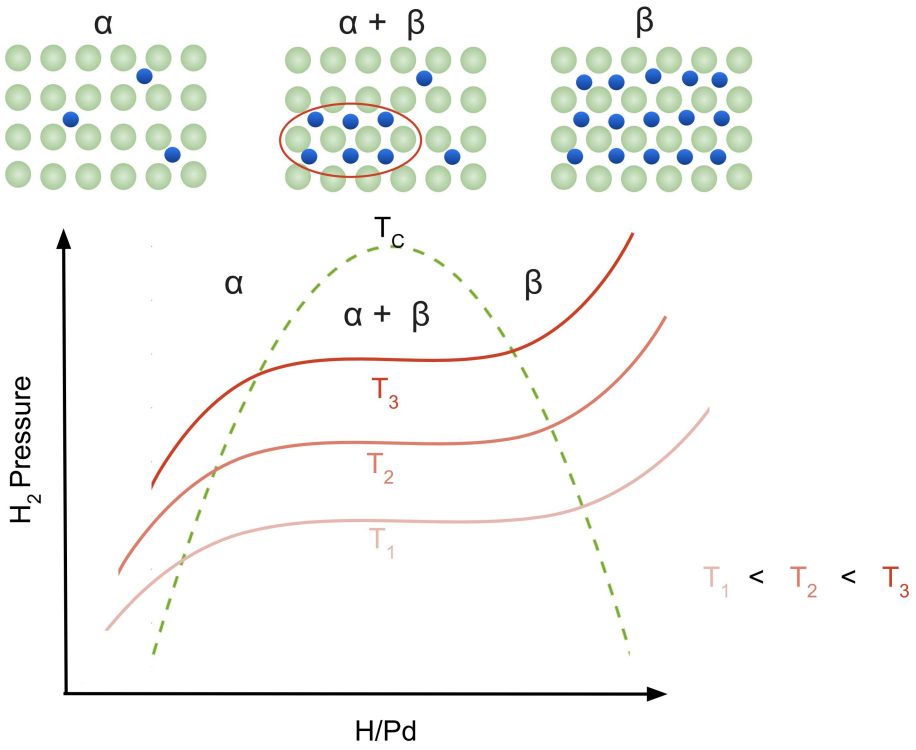

Figure 2.2: Phase diagram for PdH_x for three different temperatures (adapted from [11]). The different phases are illustrated where the α phase is a solid solution, $\alpha + \beta$ is the coexisting phase and the β phase is the metal hydride.

Pd has a FCC structure with a lattice constant of 3.887 Å, but as hydrogen is diffusing into the material, the lattice volume is increased. After the fully saturated α phase, the lattice constant is increased to 3.895 Å and during the β phase it is even further increased to 4.025 Å. The lattice expansion can be utilized for hydrogen sensing, as the lattice constant affects the optical response. However, the volume expansion also has some negative effects, as this can cause cracking and degradation in the Pd structure. [11]

The Pd-H system features hysteresis, which is the phenomenon where the pressure and H/Pd ratio relation depends on whether there is desorption or absorption of hydrogen (see figure 2.3). For a fixed temperature, the absorption pressure is always higher than the desorption pressure. Hysteresis could origin from the plastic deformation of the metal when stretching the lattice in the β phase formation. This means that there is a higher energy barrier for the phase transition of α to β in

absorption than the transition of β to α in desorption. Above T_c, where the plateau region is eliminated, there is also no hysteresis. Since the hysteresis makes the relation between pressure and H/Pd ratio nonspecific, it also has a negative influence on the performance of pure Pd hydrogen sensors.

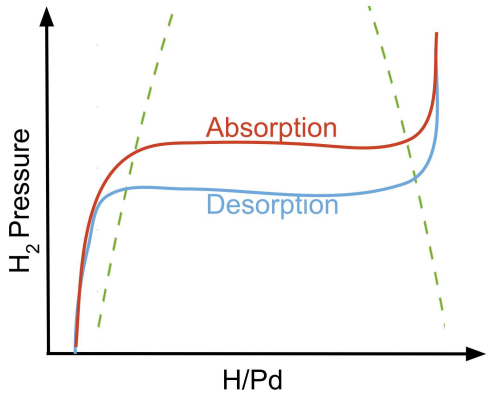

Figure 2.3: Hysteresis in the Pd hydride formation.

2.2 Localized surface plasmon resonance (LSPR)

Plasmons are the physical phenomena occurring in metals and some dielectics when applying an electromagnetic field, i.e. light. A plasmon is defined as a quantum of plasma oscillation which is the collective oscillations of the conduction electrons in the material. One specific type of plasmons is the surface plasmons that occur at the interface between the plasmonic and dielectric material. Surface plasmons are charge density fluctuations that can propagate either on a surface or locally on a nanoparticle for which it is called localized surface plasmons. When a plasmonic nanoparticle is illuminated with light with a wavelength similar to the nanoparticle size, resonance can occur where the free electrons oscillate collectively according to the electrical field of the light. At the resonant wavelength, the nanoparticle scatters or absorbs light efficiently which results in a significant peak in the extinction spectrum. [13] The phenomenon is called localized surface plasmon resonance (LSPR). An illustration of this is presented in figure 2.4.

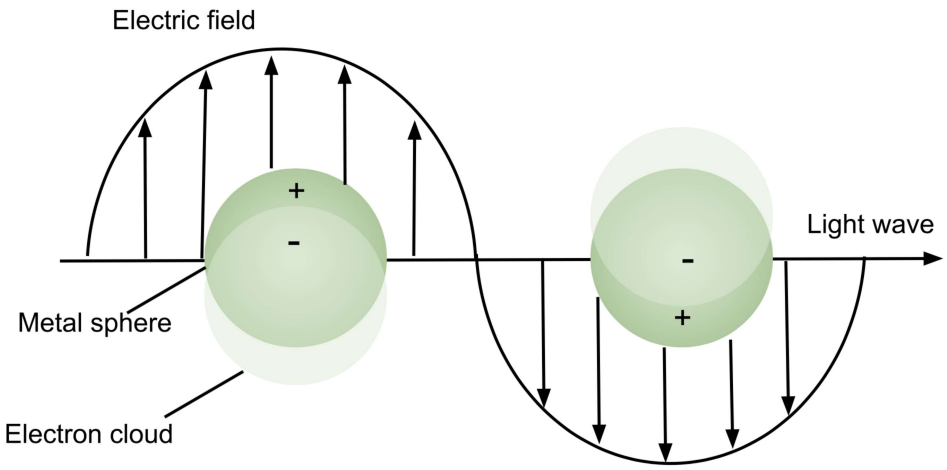

Figure 2.4: Localized surface plasmon resonance (LSPR) of a metal nanoparticle. Free electrons oscillate collectively according to the electrical field of the light.

LSPR can be understood by the Mie theory which describes the scattering and absorption of spherical metal particles. The quasi-static approximation is made meaning that the diameter of the metal sphere is assumed to be much smaller than the wavelength of the incoming light. The nanoparticle-light interaction can be described by the light absorption cross-section, σ_{abs}, light scattering cross-section, σ_{sca} and the light extinction cross-section σ_{ext}. The cross-sections for these are expressed as

$$\sigma_{ext} = \frac{18\pi\varepsilon_m^{3/2}V}{\lambda}\frac{\varepsilon_2(\lambda)}{(\varepsilon_1(\lambda)+2\varepsilon_m)^2+(\varepsilon_2)^2}, \tag{2.2}$$

$$\sigma_{sca} = \frac{32\pi^4\varepsilon_m^2V^2}{\lambda^4}\frac{(\varepsilon_1-\varepsilon_m)^2+\varepsilon_2(\lambda)^2}{(\varepsilon_1(\lambda)+2\varepsilon_m)^2+(\varepsilon_2)^2} \tag{2.3}$$

$$\sigma_{abs} = \sigma_{ext} - \sigma_{sca}, \tag{2.4}$$

where ε_m is the medium's dielectric function, V is the particle volume, λ is the wavelength of the incoming light and ε_1 and ε_2 is the real and complex part of the dielectric function. For $\varepsilon_1 = -2\varepsilon_m$, the extinction cross-section will be maximized meaning that the resonance condition is met. This will appear as the resonant peak in the extinction spectrum and is dependent on the particle material via the real part of the dielectric function and the dielectric function of the surrounding medium. The imaginary part of the dielectric function will also affect the LSPR peak in the aspect of the peak width as it is responsible for damping losses. [13] Materials such as Au and Ag are known for their low losses which results in high extinction intensities compared to Pd that suffers from higher losses [14]. From equation 2.2 one can observe that the extinction cross-section is dependent on the particle size. The particle size also strongly influences the resonance frequency where the wavelength increase with increasing particle size at the same time as the peak is broadened [15].

2.3 Pd LSPR hydrogen sensing

A highly selective hydrogen sensor can be made from hydride forming Pd nanoparticles. When the hydrogen pressure increases, the lattice expands and the permittivity of Pd changes. In turn, these two effects cause a redshift of the LSPR peak position, decrease in peak extinction and broadening of the peak [16]. The changes of the LSPR peak can be used to monitor the hydrogen concentration surrounding the Pd nanoparticle. The high surface to volume ratio of the small nanoparticles makes kinetics relatively fast and the response times of the hydrogen sensor short.

Figure 2.5a shows the LSPR peak position shift, $\Delta\lambda_{max}$, for hydrogen absorption and desorption in a pure Pd nanoparticle hydrogen sensor. The figure very much resembles the curve for hydride formation of Pd presented in figure 2.2, with a α, α to β and β phase. This means that the LSPR response has a linear relation to the absorbed hydrogen in the system. The gap between the absorption and the desorption plateau, visible in the figure, is a result of hysteresis. Hysteresis makes the peak position shift different depending on whether there is absorption or desorption and therefore makes the sensor signal nonspecific. Besides that, the hysteresis also causes degradation in the sensor, which will affect the long-term stability [17].

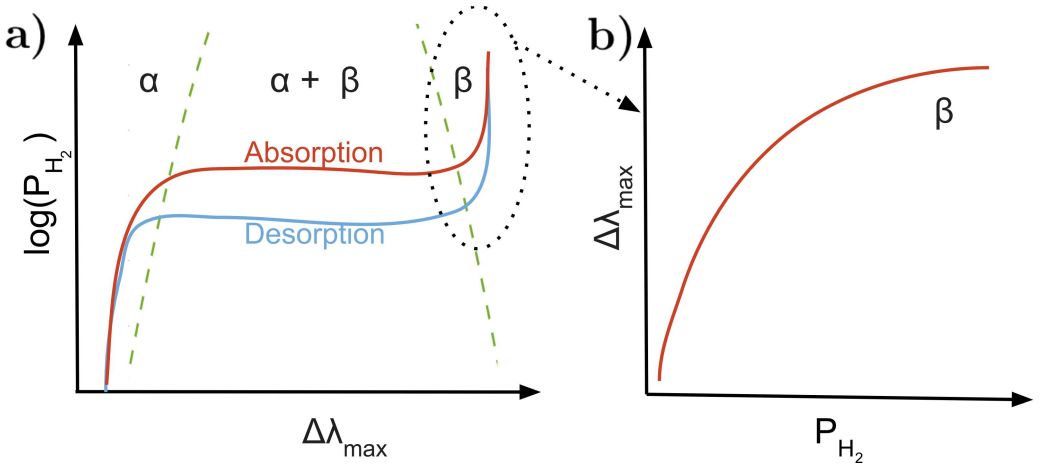

Figure 2.5: The LSPR response for hydrogen absorption and desorption in Pd nanoparticles. a) The logarithm of the hydrogen pressure as a function of LSPR peak shift. In the coexisting region, there is a gap between the absorption and desorption caused by hysteresis. b) The LSPR peak shift as a function of hydrogen pressure in the β phase. The sensitivity decreases with increasing hydrogen pressure.

To avoid the plateau region and the hysteresis, the LSPR based Pd sensor can be operated only in the α region for low pressure measurements or only in the β region for high pressure measurements. However, here the LSPR response for the pure Pd nanoparticle based hydrogen sensor is rather weak [18]. In figure 2.5a it is observable that the regions of the α and β phases provide very steep slopes. In these regions, a change in the hydrogen concentration leads to a very small change in the peak position, meaning that the sensor has low sensitivity. One should also note

that the hydrogen pressure scale is logarithmic, so that the LSPR response changes even slower at higher hydrogen pressures. This can be seen in figure 2.5b, where the peak shift is presented as a function of hydrogen pressure in the β phase.

The region of the highest sensitivity is located at the phase transition plateau. Thus, a strategy for increasing the sensitivity in a desired range is to "move" the plateau to these hydrogen pressures. This can be done by changing the temperature, since a higher temperature results in a higher plateau pressure. Another way is to alloy Pd with different metals and in this way change the material properties. The sensitivity is also affected by the LSPR peak position of the nanoparticles in the non-hydrogenated state. By redshifting the LSPR response, the sensitivity is linearly increased. This can be done by for example increasing the nanoparticle size [19].

2.4 Pd alloying for hydrogen sensing

A literature study on relevant Pd alloys and their hydrogen sensor performance is made with the purpose of finding a nanoparticle system that solves the issues with pure Pd nanoparticle based hydrogen sensing. Alloying Pd with other metals often increases the hydrogen permeability and makes the material more mechanically strong. It can also change the lattice parameters, optical properties and the critical temperature of Pd. By choosing the right alloy metal with the right content, the alloy should be optimised to act as a hydrogen sensor for low and high concentration applications respectively.

2.4.1 PdAu

As previously mentioned, gold (Au) is a metal known for its strong plasmonic response [13]. For this and many other reasons, it is often used for LSPR hydrogen sensing [18, 20]. Au has a lattice parameter of 4.0782 Å which is larger than the one for Pd [21]. Alloying Pd with Au therefore causes a pre-strain in the lattice and the volume expansion during hydride formation will not be as high. This leads to a lowered critical temperature and a mitigated hysteresis. The extinction of the LSPR peak as a function of hydrogen pressure for different levels of Au content is presented in figure 2.6 [18]. From figure 2.6a-c, it is clear that the hysteresis decreases with increasing Au content and is almost completely gone at 25 at.% Au in 30 °C. This leads to a higher accuracy ($\leq$5 % for 25 at.% Au) because of the elimination of the nonspecific response that the hysteresis provides. [18]

From figure 2.6d, a change in the slope of the LSPR response when adding Au is also visible. The less steep slope for the low pressures will lead to a better sensitivity. This is useful for the low concentration application where alloying with Au will result in a hysteresis-free, sensitive sensor [18]. Even higher alloy contents of 40 at.% Au have been used in thin-films for low concentration hydrogen sensing [22]. Within the low concentration measurement range, the sensitivity for this sensors are good and the response time short. The short response time is caused by the fact that Au strains the PdAu lattice and increases the hydrogen permeability [23].

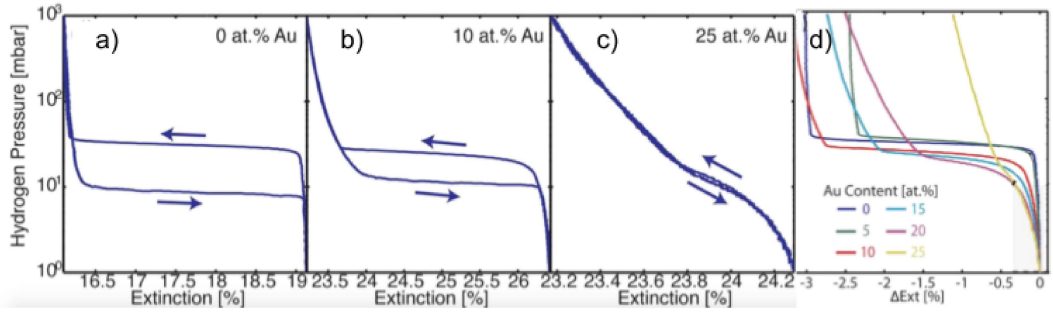

Figure 2.6: Extinction of a LSPR peak during absorption and desorption of hydrogen for a) 0 at.% Au b) 10 at.% Au and c) 25 at.% Au in PdAu alloy. d) Hydrogen absorption isotherms for six different Au contents. Figure from [18].

One should note that the total difference in extinction is not the same for all compositions. For the high concentration application, it is important to have a high sensitivity and thus a flat slope at the high pressures. For this, the highest Au content is not the most beneficial but rather a Au content of about 10-15 at.%. For the PdAu alloy with this Au content, hysteresis is still a problem. One way of solving this is issue is by increasing the temperature so that the sensor is operated above the critical temperature. An increased temperature will also move the plateau region to higher pressures and shorten the response time of the sensor. The critical temperature decreases approximately linearly with increasing Au content and for 10-15 at.% Au it is between 50-120 °C [24]. This is a much more convenient operating temperature then the critical temperature for pure Pd.

2.4.2 PdCu

Copper (Cu) is a metal with a lattice parameter smaller than Pd at 3.627 Å [25]. Alloying Pd with Cu therefore shrinks the lattice parameter and this decreases the solubility of hydrogen in the PdCu lattice. For this reason, the pressure needed for a phase transition α to β, both in the absorption and desorption, is increased. [26] Figure 2.7a shows the LSPR peak position as a function of hydrogen pressure for different Cu contents in PdCu alloys at 30 °C. At the same time as the plateau region of the curve is moved to higher pressures, the hysteresis gap decreases. [5]

When increasing the Cu content, the sensitivity for the low concentrations is decreased, as can be seen in figure 2.7b. When the plateau region is pushed to higher pressures, the initial slope is gets steeper. To eliminate the hysteresis with Cu, the content has to be $\geq$30 at.%. At this content, the sensitivity for the low concentrations is very poor. The low concentration sensor can for this reason only have a limited amount of Cu and need hysteresis elimination from another method. This could be elevation of the temperature or alloying with Au, which has been done previously [5]. However, the low concentration sensitivity will not be as good as in a PdAu alloy since the Au increases the sensitivity while Cu decreases it.

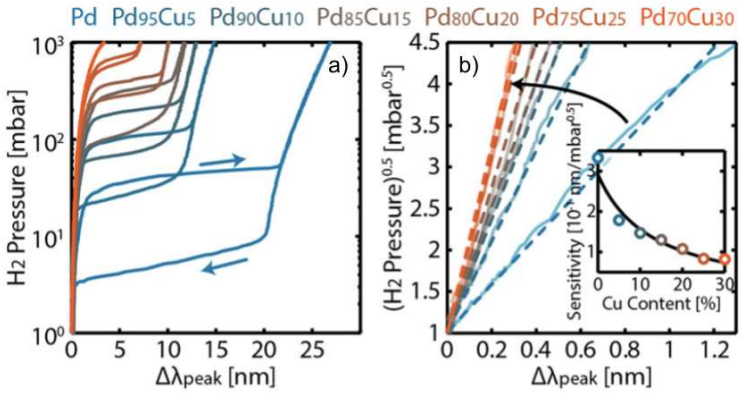

Figure 2.7: a) LSPR peak position as a function of hydrogen pressure for different Cu contents in PdCu alloy at 30 °C. b) Sensitivity for low pressures. Figure from [5].

The elevated plateau pressure is on the other hand advantageous for the high concentration sensor. By increasing the Cu content the sensitive plateau region can be moved to the measurement range of interest. In the figure, the highest measured content is 30 at.%, and this seems to result in a hysteresis-free flatter region at about 1 bar hydrogen.

Another advantage of alloying with Cu is the resistivity against poisonous molecules. By alloying Pd with as little as 5 at.% Cu, it provides protection against CO [5]. The reason for this is the weaker interaction of CO with PdCu alloy surfaces than with Pd [27]. Cu also has some resistance against sulfur, which has a good impact on the long term stability [28].

2.4.3 PdNi

Nickel (Ni) is another metal with a small lattice constant of 3.515 Å that can be used for hydrogen sensing applications. In the same way as PdCu, alloying Pd with Ni leads to a decrease in the hydrogen solubility and a suppression of the β phase [7]. The sensor performance of PdNi have previously been tested both in bulk and thin film form [29, 30]. In 2.8a, the pressure composition isotherms for various bulk PdNi alloy compositions in 25 °C is presented, while figure 2.8b shows the isotherms for various thin-film alloys in 0 °C. In this case, M and Me stands for the PdNi alloy.

From both of the isotherms it is clear that alloying Pd with Ni shifts the α to β transformation to higher pressures. For bulk PdNi with a alloy content of 13.1 at.%, the plateau region is at about 0.8 bar at room temperature [29]. One should also note that the width of the plateau changes with the Ni content in figure 2.8. The plateau first narrows with increasing Ni content and then widens. This makes the sensitive region smaller for the intermediate Ni content, which might be an issue for the sensor.

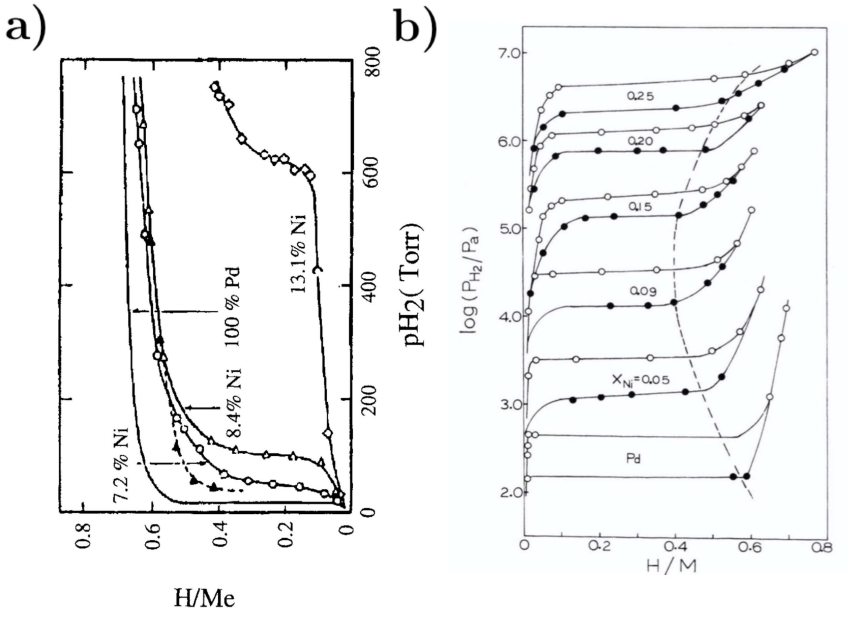

Figure 2.8: Pressure composition isotherms for different PdNi alloys. a) Bulk PdNi alloys with Ni content 7.2-13.1 at.% at 25 °C. Figure from [29]. b) Thin film PdNi alloys with Ni content 0-25 at.% at 0 °C. Figure from [30].

The influence of hysteresis is present in all compositions at the presented temperature, which can be seen in figure 2.8b. PdNi however has a special property of a strong decrease in the hysteresis when cycling. By cycling PdNi with 15 at.% Ni 7 times at 50 °C, the hysteresis disappears due to changes in the microstructure [30]. In this way, one can have a high concentration sensor that is hysteresis-free. In addition, Ni provides a decrease in the response time of approximately ten times compared to pure Pd [31]. One drawback of Ni is that the plasmonic effect is relatively low compared to Au [32]. For this reason, the LSPR peak which the hydrogen sensor relies on might be broad and difficult to analyse.

2.4.4 PdAg

Silver (Ag) has a lattice parameter of 4.086 Å and alloying Pd with Ag hence increases the lattice parameter [33]. This makes the lattice expansion during the α to β transformation decrease and the critical temperature is lowered. Above 30 at.% Ag, there is no α to β transformation in room temperature [34]. PdAg is often used for hydrogen separation membranes since Ag increases the hydrogen permeability which has its maximum at 23 at.% Ag [35]. The pressure composition isotherms for different bulk PdAg alloy compositions in 25 °C is presented in figure 2.9 [36].

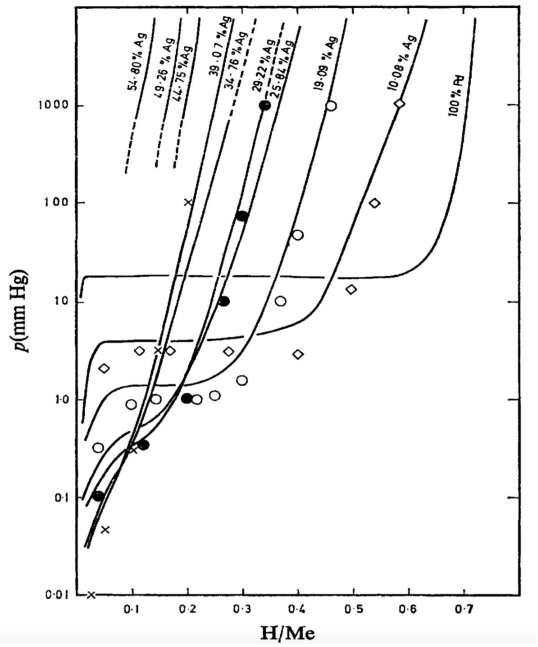

Figure 2.9: Pressure composition isotherms for different bulk PdAg alloy compositions in 25 °C. Figure from [36].

In the figure, it is observable that an increase in Ag content shifts the plateau region to lower pressures at the same time as the plateau width decreases. In a similar way as with Au, the sensitivity for hydrogen concentrations below the plateau region is enhanced with Ag. This has been used previously in a thin-film hydrogen sensor which proved that the alloy provided a stable sensor with a detection limit of 100 ppm [8]. However, the sensitivity is only increased up to a Ag content of about 25 % after which it decreases again. Since Ag has a strong plasmonic effect with low losses, the PdAg alloy has good potential for LSPR based hydrogen sensing.

2.4.5 PdBi

Another metal with an expansion effect on the Pd lattice is bismuth (Bi). Figure 2.10 shows a pressure composition isotherms for different PdBi alloy compositions in 25 °C [37]. The PdBi alloy has a similar behaviour as PdAg with a decrease in plateau pressure and plateau width with increasing Bi content. The figure indicates that the sensitivity at low concentrations is enhanced with Bi and that the highest content measured (10 at.%) would result in the highest low concentration sensitivity. For the high concentration sensitivity, Bi appears to have little impact.

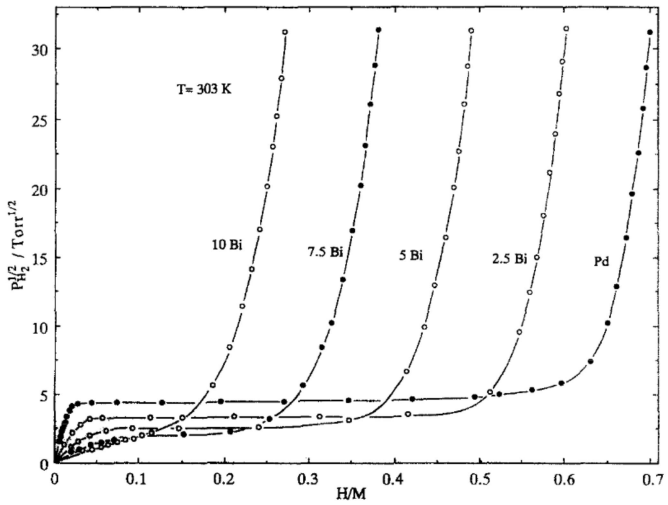

Figure 2.10: Pressure composition isotherms for PdBi with different alloy content. Figure from [37].

PdBi nanowires with a Bi content of 15 at.% has shown to have a critical temperature well below room temperature at about −70 °C [38]. The low critical temperature is an effect of the lattice expansion that Bi causes but also the geometry of the nanowires. However, the results indicate that larger nanodisks with a similar Bi content might provide a hysteresis-free hydrogen sensor at room temperature.

The most concerning issue of Bi is the weak LSPR response. The absorption spectrum for Bi nanoparticles have shown small plasmonic resonances around the UV region [39]. However, this response might not be sufficient for LSPR based hydrogen sensing.

3

Sensor composition suggestions

As the scope of the thesis is limited, not all of the Pd alloys from the literature study can be analyzed. A decision on the most interesting nanoparticle systems for fuel cell as well as safety applications is made and the suggested alloys are presented in table 3.1. Motivations of the suggestions is further clarified in the following sections.

Application	Alloy	Alloy content	Temperatue
Fuel cell	PdNi	15 at.%	30 °C
Fuel cell	PdCu	30 at.%	30 °C
Fuel cell	PdCu	40 at.%	30 °C
Safety	PdAg	20 at.%	80 °C
Safety	PdAg	30 at.%	30 °C

Table 3.1: Suggested nanoparticle systems for high and low hydrogen concentration applications.

3.1 PdNi

Ni has an increasing effect on the phase transition plateau pressure. Previous measurements indicate that 13.1 at.% Ni gives a plateau pressure of about 0.9 bar. This means that an alloy with 15 at.% Ni can result in a sensor with high sensitivity around 1 bar, or 100 % hydrogen in ambient pressure. The alloy is therefore suitable for fuel cell applications. Hysteresis is not expected to be eliminated for this alloy which might be an issue for the sensor performance. The temperature chosen for this sensor is 30 °C and it should be tested with Ar as background gas, as this is an inert gas.

3.2 PdCu

Also Cu increases the plateau pressure of Pd. With 30 at.% Cu, the plateau appears to be at around 1 bar. Therefore the PdCu alloy of this content is expected to have good performance for high hydrogen concentrations. By increasing the Cu content even higher to 40 at.% an hypothesis is that the region with good sensitivity could be further elevated to higher pressures. For this reason also an alloy with 40 at.% Cu should be tested. With these alloys, hysteresis is expected to be eliminated and the sensors can be operated at 30 °C. Also here the test should be conducted in Ar.

3.3 PdAg

Ag has a decreasing effect on the phase transition plateau pressure. A PdAg alloy with 30 % Ag would be suitable for a low concentration hydrogen sensor with a high sensitivity and low hysteresis. Also 20 at.% Ag would result in a high sensitivity for low concentrations, but here hysteresis is an issue. To solve this, the sensor could be operated above the critical temperature. For thin-film PdAg with 10 at.% Ag, the critical temperature is somewhere around 100 °C [40]. Since the critical temperature is known to decrease with increasing Ag content, a rough estimate of the critical temperature for 20 % Ag would be less than 80 °C. The $Pd_{70}Ag_{30}$ alloy should therefore be tested in 80 °C, while the $Pd_{80}Ag_{20}$ alloy can be tested in 30 °C. However one should note that increasing the temperature will increase the plateau pressure and thus take away some of the effect that Ag has. The measurements should be made with air as the background gas.

4
Methods

The suggested nanoparticle alloys are fabricated by the method of hole-mask colloidal lithography (HCL). Their performance is then evaluated by two different hydrogen sensing test set-ups. In the following chapter, the methods used for sensor chip manufacturing as well as the set-ups used for sensor characterization are presented.

4.1 Sensor chip manufacturing

The method of (HCL) is used to make nanodisk sensor chips. HCL is a bottom-up nanofabrication method that utilizes colloidal polystyrene (PS) nanobeads that self-assemble to create a mask. By performing material deposition through the mask, nanostructures are fabricated. HCL is effective on large areas and versatile when it comes to structures and materials. For this reason, it is a suitable method for sensor fabrication. The HCL process is presented in figure 4.1 and the method will be briefly presented in the following section. For an in-depth description of the HCL process, refer to [41].

The mask is made by first cleaning a substrate of fused silica with isopropanol (IPA), acetone, methanol, and then IPA again in an ultrasonicator. Then, a Poly(methyl methacrylate) (PMMA) layer is deposited by spin-coating where a few drops of PMMA are applied and then spun at 2000 rpm so that it forms a 200 nm thick layer. The substrate is soft-baked to evaporate excess solvent before it is exposed to oxygen plasma to reduce surface hydrophobocity. On top of the PMMA layer, positively charged poly(diallyldimethylammonium chloride) (PDDA) solution is drop-coated. This is incubated for 1 min after which it is washed with Milli-Q water and dried with N_2 gas. A solution of negatively charged PS nanobeads with a diameter 210 nm is drop cast on the positive surface and incubated for 2 min. In this way, the PS beads self assemble and form a monolayer on the substrate which then is cleaned with Milli-Q water and dried with N_2 gas. E-beam physical vapor deposition (PVD) is used to deposit a 15 nm layer of chromium. After this, the PS beads are stripped off by a tape so that the substrate now is a Cr mask with holes down to the PMMA layer. Oxygen plasma etching is utilized to transfer the hole pattern of the Cr mask to the PMMA layer. From this hole-mask, nanodisks can be fabricated. This is done by first deposing Pd on the substrate and then deposing the desired alloy metal on top of this using e-beam PVD. The final step is to remove the mask by dissolving it in Acetone. To transform the Pd and alloy metal bilayer to a homogeneous alloy, the nanodisks are annealed. The sensor chips are annealed in reducing atmosphere

(4 % hydrogen in Ar) with 150 ml/min, at 500 °C for 24 h.

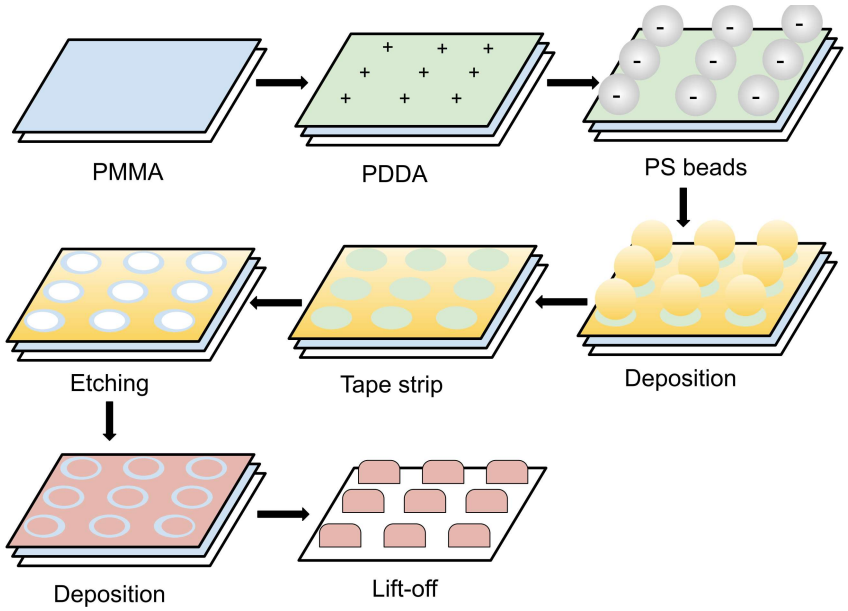

Figure 4.1: Hole-mask colloidal lithography (HCL) nanofabrication process, adapted from [42].

By this method, sensor chips of 1x1 cm with nanodisks of diameter 210 nm and thickness 25 nm are made. The compositions fabricated are pure Pd, $Pd_{85}Ni_{15}$, $Pd_{70}Cu_{30}$, $Pd_{60}Cu_{40}$, $Pd_{80}Ag_{20}$ and $Pd_{70}Ag_{30}$. All the nanofabrication is conducted in Chalmers cleanroom facility.

4.2 Pressure composition isotherm measurements in vacuum apparatus

The pressure composition isotherms of the nanodisk sensor chips are measured in a vacuum apparatus which is illustrated in figure 4.2. The sensor is placed in a vacuum chamber with ports for incoming light from a polychromatic halogen light source and transmitted light to a UV-visible fixed-grating spectrophotometer. A thermocouple wire is attached in contact with the sensor chip and monitors the sensor temperature. A resistive heating coil connected to a DC-power supply surrounds the vacuum chamber. The sensor temperature can be controlled by the DC-power supply that is connected in a feedback-loop manner with the thermocouple.

The vacuum chamber is connected to a 100 % hydrogen reservoir and a Pfeiffer Turbomolecular Pump. The hydrogen pressure in the chamber is controlled by leak and switch valves on the reservoir and vacuum pump side. The pressure in the chamber is measured by two capacitance manometers of resolution 1-1000 µbar and 1-1000 mbar.

The pressure composition isotherms are initiated by placing the sensor in the vacuum chamber and letting the sensor temperature stabilize to the desired value. After that the sensor is flushed with high concentrations of hydrogen five times in order to stabilize the sensor. The absorption isotherm are then made by slowly increasing the pressure by opening the leak valve on the hydrogen reservoir side while measuring the LSPR peak position. When the pressure is 1 bar, the reservoir valve is closed and the desorption isotherm is measured by slowly decreasing the pressure by opening the leak valve to the vacuum pump. Due to the safety concerns that comes with high pressures of hydrogen and the limitations in the setup, only pressures between 0 and 1 bar can be measured.

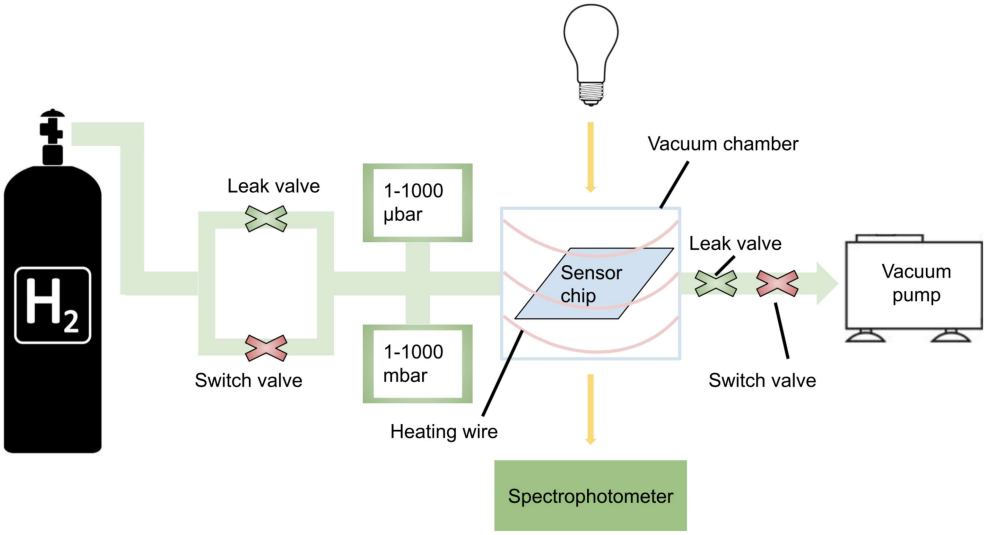

Figure 4.2: Schematic drawing of the vacuum apparatus for pressure composition isotherm measurements.

4.3 Hydrogen sensing tests in Insplorion X1 reactor

The sensor performances of the Pd alloy nanodisk sensors such as kinetics, sensitivity and limit of detection are evaluated by measurements in an Insplorion X1 flow reactor. In figure 4.3, the scheme of the reactor is presented. Two sensors are mounted in a quartz tube reactor chamber where they are illuminated by a halogen light source via an optical fiber and an optical collimator. The transmitted light is connected via an optical collimator and an optical fiber to a UV-visible spectrophotometer. The Insplorer software monitors the optical response and performs a real-time data fitting to record the optical descriptors such as peak and centroid position. A DC power supply is connected to a resistive heating coil that is wrapped around the quartz tube. The temperature is controlled in a feedback-loop manner by a PID thermocontroller with a K-type thermocoupler in contact with one of the sensor chips.

The gas mixture flowing through the reactor with the rate 200 ml/min is controlled using mass flow controllers (MFCs). The MFCs are in turn controlled by a LabVIEW program that is set to provide certain concentrations at different times. All tests are initiated by flushing the sensor chips with 100 % hydrogen five times. In the fuel cell application tests, 5 min pulses of increasing concentrations 5-95 % hydrogen in Ar are then applied. To get these concentrations, one MFC is connected to 100 % hydrogen and another one to 100 % Ar. In the safety application test, 30 min pulses of increasing concentrations 0.062-5.52 % hydrogen in synthetic air are used. To get these concentrations, one MFC is connected to synthetic air and two MFCs of different maximum flow are connected to 25 % hydrogen. The reason for this is to cover the entire range without exceeding the maximum flow of any MFC.

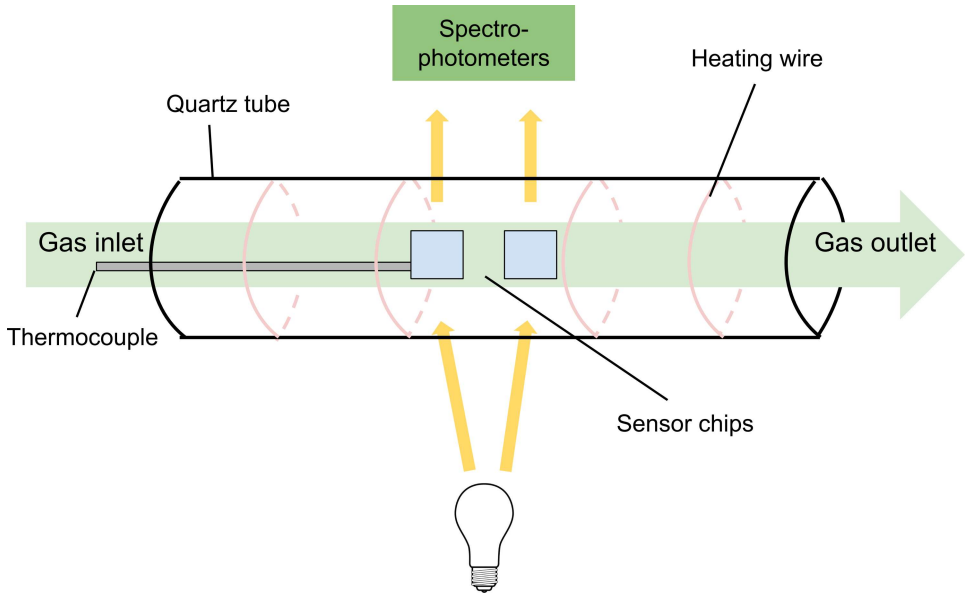

Figure 4.3: Insplorion X1 flow reactor.

5
Results and Discussions

The following chapter presents the hydrogen sensor characteristics of the three different types of alloys. The two first sections cover the PdNi and the PdCu alloys for fuel cell applications, while the third includes the PdAg alloy for safety applications. Results from the vacuum apparatus and X1 reactor measurements are presented, and from this relevant hydrogen sensing properties are calculated. Together with this, a discussion of the results and their implications is included.

5.1 PdNi alloy for fuel cell applications

For the fuel cell application, the sensor performance of the $Pd_{85}Ni_{15}$ alloy for high hydrogen concentrations is investigated. The sensor characteristics is measured in the X1 reactor and the vacuum apparatus and the results are presented in figure 5.1.

Figure 5.1a shows the pressure composition isotherm for the PdNi alloy at 30 °C for 0-1 bar. The figure shows measurement points for absorption of hydrogen in red and desorption of hydrogen in green as well as fitted lines of the same colour as guide for the eye. The characteristic phase transition plateau starts at around 300 mbar and continues well above the measurement range. At the plateau, the desportion pressure is slightly lower than the absorption pressure which could be an indication of hysteresis. Nevertheless, the fact that the plateau extends above the measurements range indicates that there is still some α-phase left at 1 bar. For this reason, the full effect of hysteresis cannot be examined from this measurement. The phase transition plateau of PdNi can be compared to the one for pure Pd nanodisks shown in the pressure composition isotherm in figure 5.2a. Here the absorption plateau is at 25-40 mbar and the desorption plateau at 7-10 mbar. Thus, the plateau pressure for Pd increases significantly with the addition of Ni in accordance with the hypothesis. The smaller lattice constant of Ni makes the pressure needed for α to β transition increase which is seen as a higher plateau pressure in the isotherm. However, at first sight the plateau seems to be located at lower pressures than for previous measurements of bulk and thin film PdNi of similar composition [29, 30]. But, since the vacuum apparatus is limited to 1 bar, the full plateau cannot be seen from these measurements. For this reason it is hard to define the starting point of the plateau, and the result might actually be in line with the reported values.

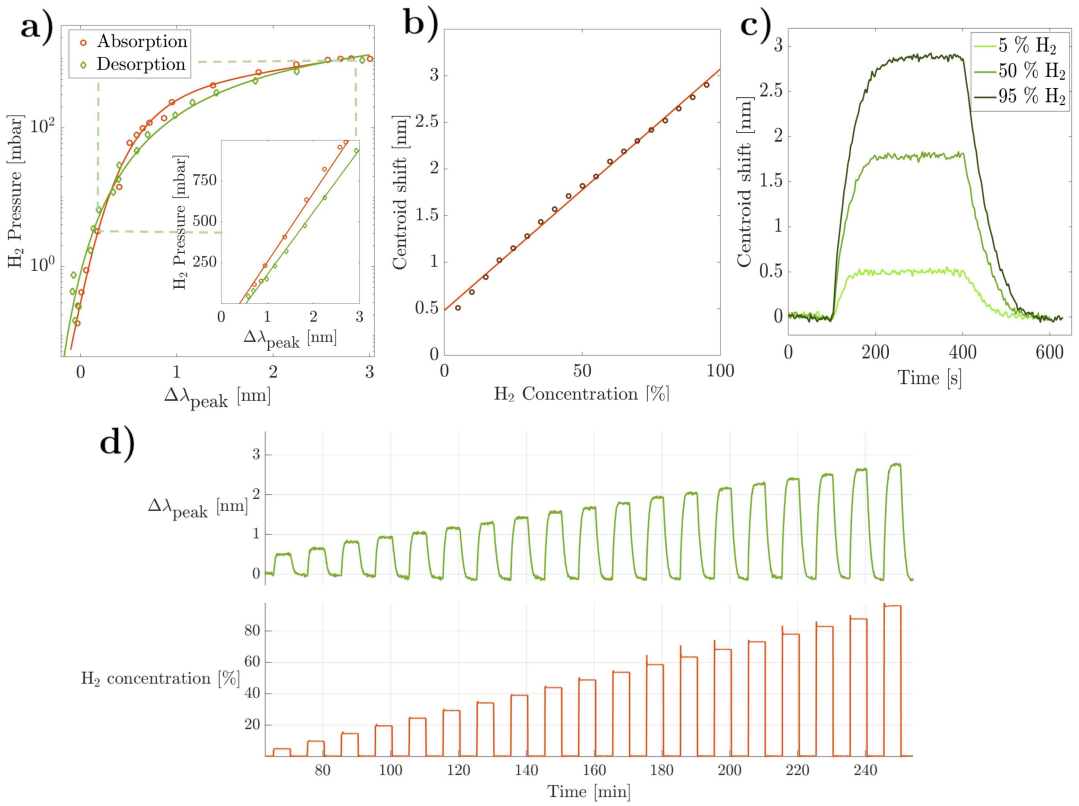

Figure 5.1: Sensor characteristics for $Pd_{85}Ni_{15}$. a) Pressure composition isotherm for 0-1 bar at 30 °C. The phase transition plateau starts at around 300 mbar and continues above 1 bar. b) Sensor response for 5-95 % hydrogen in 30 °C. A line with slope 0.026 nm/% is fitted to the measurement points. c) Sensor kinetics for 5, 50 and 95 % hydrogen. d) X1 measurements for 5-95 % hydrogen in 30 °C with Ar as background gas.

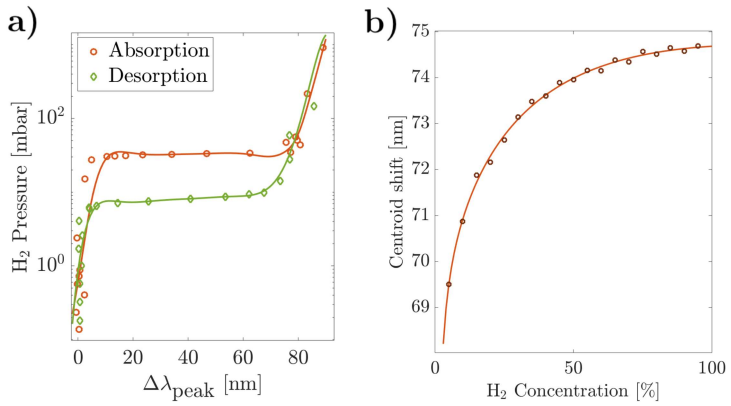

Figure 5.2: Sensor characteristics for pure Pd. a) Pressure composition isotherm for 0-1 bar at 30 °C. b) Sensor response for 5-95 % hydrogen in 30 °C with Ar as background gas.

From the PdNi pressure composition isotherm, the alloy appears well suited for high concentration sensing. To further look into the sensitivity and kinetics of the sensor, the $Pd_{85}Ni_{15}$ sensor chip is tested for high hydrogen concentrations 5-95 % in an X1 measurement at 30 °C with Ar as background gas. The result is presented in figure 5.1d. The centroid position is here used as the sensor signal due to its stability. For all concentrations the centroid shifts significantly from its original position 713 nm with a maximum response of 2.9 nm at 95 % hydrogen. There is a small drift in the baseline of about -0.2 nm during the measurement. The centroid position changes nearly linearly with hydrogen concentration which can be seen in figure 5.1b. This aligns with the result from the isotherm measurement where the peak position changes linearly with hydrogen pressure above 50 mbar. The slope of the line corresponds to the sensitivity and is determined to 0.026 nm/%. By comparing the sensitivity to the noise in the sensor signal, a measure of the sensor precision in the range 5-95 % hydrogen can be calculated. The standard deviation of the noise, σ, is 0.024 nm which means that with the sensor has a 3σ precision of 2.8 %.

For concentrations <5 % hydrogen, the peak position does no longer change linearly with the hydrogen concentration. This can be seen in figure 5.1a but also from the fact that the fitted line in figure 5.1b does not pass through the origin. The sensitivity in this region is higher than in the 0.026 nm/% reported for larger concentrations. A rough estimate of the limit of detection is made by comparing the sensitivity in the low hydrogen region with the noise. This results in a limit of detection of 0.71 % which is well below the desired value for the fuel cell application.

The sensor response of PdNi can be compared to the response of the pure Pd nanodisk sensor presented in figure 5.2b. The Pd sensor is tested for the same concentrations 5-95 % hydrogen at 30 °C with Ar as background gas. For all concentrations, there is a large centroid shift from the original centroid position of 703 nm to around 775 nm, but as the concentration increase, the sensitivity decrease. At 30 % hydrogen, the precision is above 5 % and the sensor is no longer useful. For this reason, PdNi is a more beneficial material for fuel cell applications as the sensitivity is constant even at concentrations up to 95 %. If the high pressure isotherm of the nanodisk PdNi is in line with previous meassurements of bulk and thin-film, the alloy will provide good sensitivity also for higher pressures than 1 bar.

The response times for the sensors are analyzed from the kinetics of the X1 measurements presented in figure 5.1c. The response times for 90 % signal (t_{90}) are 36 s for 5 % hydrogen, 64 s for 50 % and 84 s for 95 %. The recovery times for 10 % signal (t_{10}) are slightly higher at 72 s for 5 %, 97 s for 50 % and 109 s for 95 %. Comparing to the pure Pd nanoplasmonic sensor with response times 30 s for 5 %, 17 s for 50 % and 15 s for 95 %, the kinetics is slower for the PdNi sensor. In addition, the response times increase with increasing concentration which is the opposite of the behaviour for pure Pd. One explanation for the slow kinetics could be that the measurement range is within the coexisting phase region of PdNi while it is in the β-phase for Pd. Especially at the two higher concentrations 50 % and 95 %, the isotherm shows indications that the phase transition has begun. The α to β phase transition is known to be the slowest step in the absorption process and therefore causes long response times [43].

5.2 PdCu alloys for fuel cell applications

PdCu alloys with compositions $Pd_{70}Cu_{30}$ and $Pd_{60}Cu_{40}$ are tested for high hydrogen concentrations with the purpose of fuel cell monitoring. The sensor characteristics for the $Pd_{70}Cu_{30}$ alloy is tested by the vacuum apparatus and the X1 reactor and the results are presented in figure 5.3. Figure 5.3a shows the pressure composition isotherm for 0-1 bar in 30 °C. The phase transition plateau starts at around 200 mbar and continues past the measurement range. In accordance with previous measurements on the same composition, the peak position shifts approximately 4 nm with 1 bar hydrogen [5]. Compared to the isotherm of pure Pd presented in figure 5.2a, the plateau pressure is clearly increased and the hysteresis seems to be mitigated, even though this cannot be completely determined due to the remaining α-phase at 1 bar.

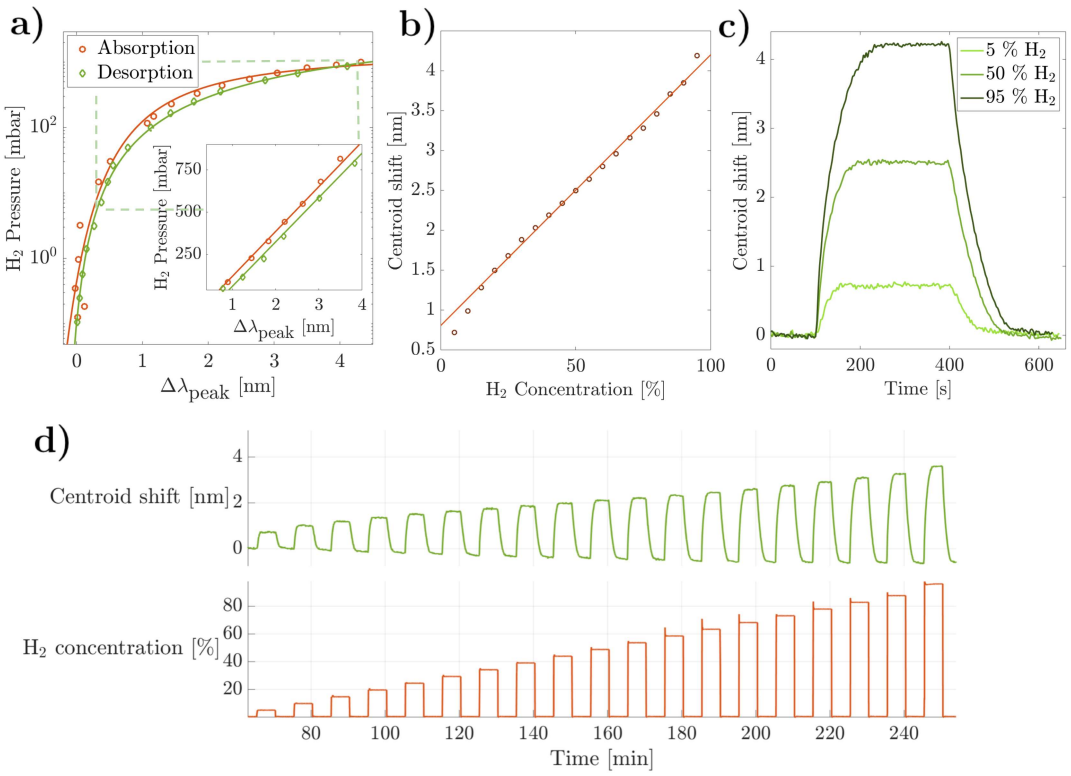

Figure 5.3: Sensor characteristics for $Pd_{70}Cu_{30}$. a) Pressure composition isotherm for 0-1 bar at 30 °C. The phase transition plateau starts at around 200 mbar and continues above 1 bar. b) Sensor response for 5-95 % hydrogen in 30 °C. A line with slope 0.035 nm/% is fitted to the measurement points. c) Sensor kinetics for 5, 50 and 95 % hydrogen. d) X1 measurements for 5-95 % hydrogen in 30 °C with Ar as background gas.

Figure 5.3d shows the results from the X1 measurement with hydrogen concentrations 5-95 % at 30 °C with Ar as background gas. There is a significant response for all concentration with a maximum centroid shift of 4.2 nm at 95 % hydrogen from

the original centroid position 650 nm. The baseline has a drift of about −0.6 nm, which is slightly more than for PdNi. In figure 5.3b the nearly linear dependence of the sensor response for PdCu is presented. A line with slope/sensitivity 0.035 nm/% is fitted to the data points and the precision is calculated to 1.7 % for the measured interval. The limit of detection is estimated to 0.41 %. From this it is evident that the PdCu alloy has better potential for high concentration measurements compared to the pure Pd. This results also suggests that PdCu might have better sensor properties than PdNi when it comes to sensitivity, precision and limit of detection.

The kinetics of the $Pd_{70}Cu_{30}$ sensor is presented in figure 5.3c. The response times, t_{90}, are 51 s for 5 % hydrogen, 59 s for 50 % and 87 s for 95 % while the recovery times, t_{10}, are 61 s for 5 % hydrogen, 92 s for 50 % and 104 s for 95 %. This is similar to the kinetics of PdNi but slower than for Pd. Since the measurement interval for PdCu is within the phase transition region, the α to β transformation might be the reason for the longer response times also for this alloy.

Also for $Pd_{60}Cu_{40}$, the pressure composition isotherm is measured and the results is presented in figure 5.4. The isotherm is very similar to the one for $Pd_{70}Cu_{30}$ with a plateau pressure of around 200 mbar and a peak position shift of 4 nm at 1 bar. As the higher content copper is expected to have a better performance at >1 bar, measurements with higher pressures are needed to further investigate its benefits. For this reason, only the $Pd_{70}Cu_{30}$ alloy was analyzed in the X1 reactor.

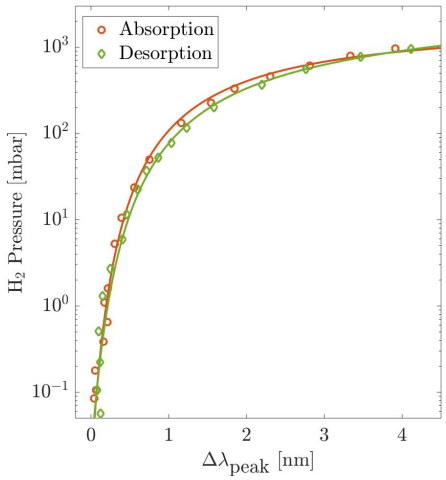

Figure 5.4: Pressure composition isotherm of $Pd_{60}Cu_{40}$ for 0-1 bar at 30 °C. The phase transition plateau starts at around 200 mbar and continues above 1 bar.

5.3 PdAg alloys for safety applications

For safety applications, the PdAg alloys are tested on their low concentration hydrogen sensing properties. The sensor characteristics of the low content alloy, $Pd_{80}Ag_{20}$, at the elevated temperature 80 °C is presented in figure 5.5. Figure 5.5a shows the pressure composition isotherm at 0-1 bar in 80 °C. The curve has a characteristic shape with a phase transition plateau at around 15-80 mbar which is similar to the

plateau pressure of pure Pd in 30 °C. Since the temperature increases the plateau pressure, it is safe to assume that Ag have a lowering effect of the plateau pressure as expected. For this elevated temperature there is, as expected, little signs of hysteresis.

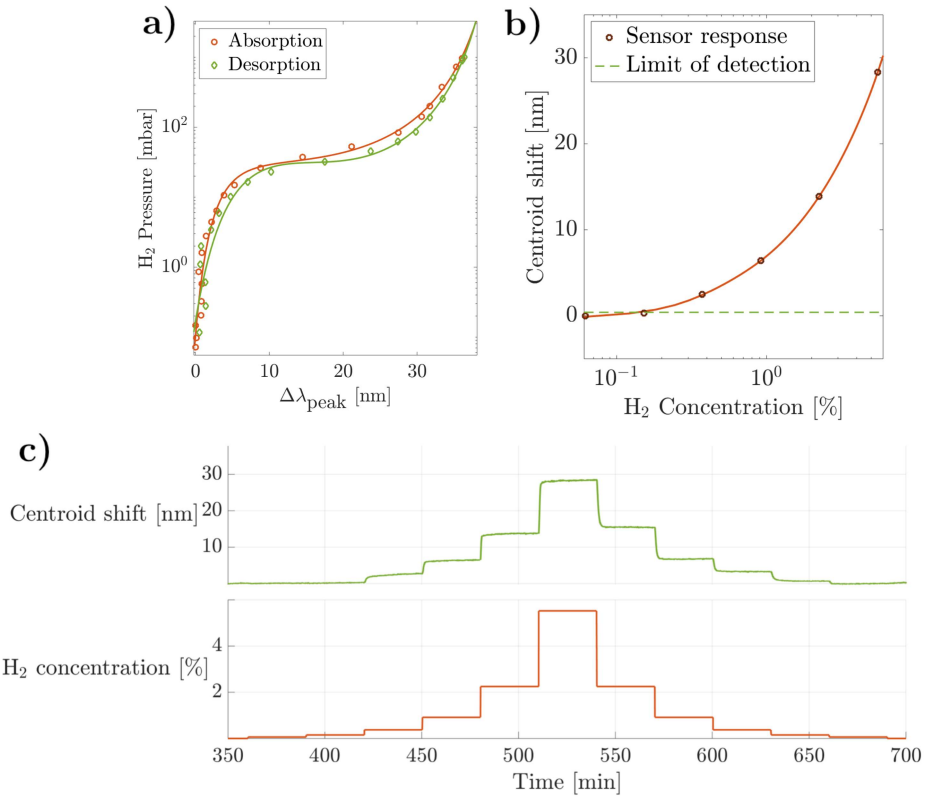

Figure 5.5: Sensor characteristics for $Pd_{80}Ag_{20}$. a) Pressure composition isotherm for 0-1 bar at 80 °C. There is a phase transition plateau at around 15-80 mbar. b) Sensor response for 0.062-5.52 % hydrogen in 80 °C. The limit of detection is 0.20 %. c) X1 measurements for 0.062-5.52 % hydrogen in 80 °C with air as background gas.

To further investigate the sensitivity, kinetics and tolerance to ambient conditions of the sensor, an X1 measurement is made. Figure 5.5c presents the results from this measurement with concentrations 0.062 %-5.52 % at 80 °C with synthetic air as background gas. The concentrations are changed with logarithmic intervals as the sensor response is expected to follow this pattern. From the figure one can observe that only concentrations $\geq$0.37 % causes a change in the centroid position. The maximum shift from the non-hydrided centroid peak of 720 nm is measured to 28 nm. In figure 5.5b, the centroid shift is plotted against hydrogen concentration. The shape of the curve aligns with the results from the isotherm measurements with large responses above 1.5 % or 15 mbar hydrogen. By comparing the sensor response to 3σ of the noise, the limit of detection is calculated to 0.20 %. Above 1 % hydrogen concentration, the sensitivity is almost constant at around 5 nm/% with the high precision of 0.06 % but in the interval 0.37-0.91 % the sensitivity has its highest value of 7.2 nm/% with precision 0.04 %.

For comparison, a pure Pd sensor is tested in an X1 measurement under the same conditions as the $Pd_{80}Ag_{20}$ sensor. The sensor response is presented in figure 5.6 together with a fitted line. In the figure it is clear that all measurement points except the first one is above the limit of detection which is determined to 0.083 %. The maximum response is however not very high at 3.3 nm, compared to the 28 nm reported for the low alloy content PdAg. This is also seen in the lower sensitivity of approximately 0.5 nm/% around 1 % hydrogen with the precision 0.35 %. Thus, the measurements suggests that Ag decreases the plateau pressure of Pd and the sensitive region is moved to around 1 %, which could be beneficial for safety applications.

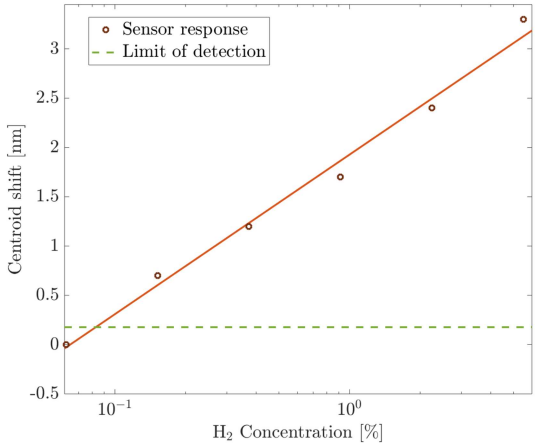

Figure 5.6: Sensor response for pure Pd for 0.062-5.52 % hydrogen in 80 °C with air as background gas. The limit of detection is calculated to 0.083 %.

With the purpose of further decreasing the plateau pressure and in this way moving the sensitive region to even lower concentrations, a higher alloy content of 30 at.% Ag is investigated. The sensor characteristics is presented in figure 5.7. Even though the $Pd_{70}Ag_{30}$ alloy is expected to be hysteresis-free at room temperature, an elevated temperature of 80 °C is chosen for the measurements for the cause of kinetics. This issue will be revisited in a later section.

The pressure composition isotherm of $Pd_{70}Ag_{30}$ at 80 °C is presented in figure 5.7a. The plateau, that is a little less significant than in the lower content alloy, starts at around 5 mbar and goes up to 50 mbar. For this alloy, there seems to be an unexpected effect of hysteresis. However, the slow kinetics of the alloy makes the isotherm measurements not fully reliable. Figure 5.7c shows the results from the X1 measurements of $Pd_{70}Ag_{30}$ for concentrations 0.062 %-5.52 % at 80 °C with synthetic air as background gas. The maximum centroid shift from 734 nm to 770 nm, is higher then for the lower content alloy but the low concentration response is smaller. Figure 5.7b presents the X1 sensor response together with a fitted curve. The shape of the curve somewhat resembles the one in figure 5.7a with largest sensitivity for 0.5-5 % hydrogen, which corresponds to the plateau region of the isotherm. Above 5 % hydrogen, the sensitivity appears to decrease. The limit of detection is determined to 0.38 %, which is just above the third measurement point. The sensitivity around 0.92-2.25 % is as high as 16.8 nm/% with a good precision of 0.02 %.

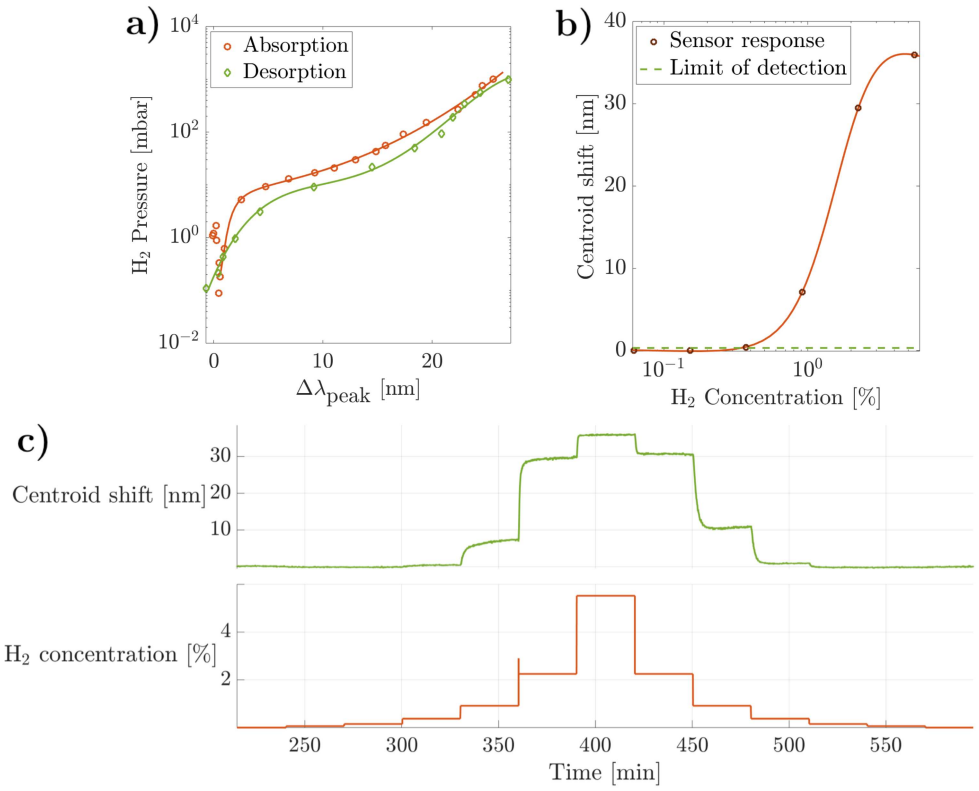

Figure 5.7: Sensor characteristics for $Pd_{70}Ag_{30}$. a) Pressure composition isotherm for 0-1 bar at 80 °C. There is a phase transition plateau at around 5-50 mbar. b) Sensor response for 0.062-5.52 % hydrogen in 80 °C. The limit of detection is 0.38 %. c) X1 measurements for 0.062-5.52 % hydrogen in 80 °C with air as background gas.

A comparison of the sensor responses for $Pd_{80}Ag_{20}$ and $Pd_{70}Ag_{30}$ is presented in figure 5.8. $Pd_{80}Ag_{20}$ is presented in red and $Pd_{70}Ag_{30}$ in green. From the figure, it is observable that the high content alloy results in a sensor with a higher sensitivity (seen by the larger slope) in the 1 % hydrogen region and larger response above 2 %, compared to the low content alloy. However, the range of high sensitivity is smaller for $Pd_{70}Ag_{30}$ than for $Pd_{80}Ag_{20}$. This smaller range can also be seen in the isotherms of PdAg where $Pd_{70}Ag_{30}$ has a more narrow plateau than $Pd_{80}Ag_{20}$. The hypothesis that $Pd_{70}Ag_{30}$ would move the sensitive region to lower concentrations and thus lower the limit of detection, proved to be inaccurate. For this reason, $Pd_{80}Ag_{20}$ can be seen as the alloy with the better sensor performance of the two, with a wider range of high sensitivity and a lower limit of detection. To be able to reach even lower limits of detection, further increasing the alloy content of PdAg is not the way. For this cause it might be interesting to look into other alloy metals such as Bi.

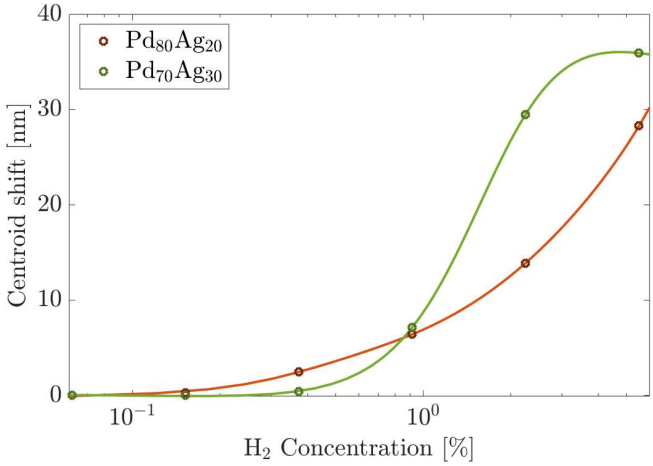

Figure 5.8: Sensor response for $Pd_{80}Ag_{20}$ (red) and $Pd_{70}Ag_{30}$ (green) for 0.062-5.52 % hydrogen in 80 °C.

Response times for both of the PdAg sensors as well as the pure Pd sensor in 80 °C are presented in table 5.1. There is an expected behaviour of decreasing response times with increasing hydrogen concentrations for all sensor chips. The response times for the both Ag alloys are significantly longer than the ones for pure Pd. One explanation of the slow kinetics could be the α to β phase transition that occurs in the measurement region for both $Pd_{80}Ag_{20}$ and $Pd_{70}Ag_{30}$, but above the measurement region for Pd. For low concentrations $Pd_{70}Ag_{30}$ is slower than $Pd_{80}Ag_{20}$ but for the highest concentration, it is faster. This aligns with the fact that the high content alloy is in the β phase above 5 % hydrogen. Another reason could be that the hydrogen diffusion coefficient is known to decrease with increasing Ag content at the same time as the activation energy increases [44].

As the kinetics increases for increasing temperature, the response times is very much longer at room temperature. The slow kinetics becomes a problem both in the isotherm and the X1 measurements. At 30 °C, the pressure in the vacuum apparatus have to be changed so slow that it is inconvenient. For this reason, only the elevated temperature was used in the sensor tests.

H_2	t_{90} $Pd_{80}Ag_{20}$	t_{90} $Pd_{70}Ag_{30}$	t_{90} Pd
0.15 %	-	-	54 s
0.37 %	426 s	-	36 s
0.92 %	138 s	270 s	30 s
2.23 %	54 s	126 s	30 s
5.52 %	48 s	36 s	24 s

Table 5.1: Response times, t_{90}, for $Pd_{80}Ag_{20}$, $Pd_{70}Ag_{30}$ and pure Pd in 80 °C.

6
Conclusion and Outlook

In this study, an investigation of nanoplasmonic hydrogen sensing properties connected to the nanoparticle composition has been made. The results confirmed that the sensitive region of a nanoplasmonic sensor can be tuned by alloying Pd with other metals. Metals such as Ag, that has a larger lattice parameter than Pd, can increase the low concentration sensitivity and is therefore suited for safety applications. Both of the tested alloys, $Pd_{80}Ag_{20}$ and $Pd_{70}Ag_{30}$, showed increased sensitivity compared to pure Pd near 1 % hydrogen. However, they also had a higher limit of detection and significantly slower kinetics.

The study showed that metals such as Ni and Cu, that have smaller lattice parameters than Pd, increase the high concentration sensitivity. Both PdNi and PdCu demonstrated good potential for fuel cell monitoring applications with linear relations between hydrogen concentration and sensor response in the range 5-95 %. The sensitivities were calculated to 0.026 nm/% and 0.035 nm/% respectively. The sensitivity, precision and limit of detection of PdCu was slightly better than for PdNi and the kinetics for both of the sensors were slower than for the pure Pd nanoparticle sensor.

There is a need for further investigation before nanoplasmonic hydrogen sensors for fuel cell and safety applications can be made. For the low hydrogen concentration applications, more research to find the optimal alloy is needed. PdAu has previously proven to be a good candidate, but it would also be interesting to evaluate the performance of PdBi. For safety applications, there is a demand for high robustness towards humidity, poisoning and changed temperature. Also to improve kinetics of the sensor is crucial, as the target response time is <1 s. An improvement of both the robustness and the kinetics can be made by coating the nanodisk with a polymer.

Due to limitations in the set-up, only pressures <1 bar could be tested. In future studies, it is of interest to see how PdNi and both of the PdCu alloys perform at higher pressures 1-3 bar. The pressure composition isotherms from previous measurements indicate that the sensitive region might continue well above 1 bar, but this is yet to be tested for the nanoparticle alloys. Also, in a higher pressure measurement, the full effect of hysteresis will be observable. A hypothesis is that the PdCu alloys will show less hysteresis than PdNi and therefore have a better sensor performance. The response times for both of the sensors were long, and it would be interesting to look deeper into the reason for this and further analyze this behaviour. Another property that has to be investigated also for fuel cell applications is the resistivity towards humidity.

Bibliography

[1] Andreas Züttel et al. "Hydrogen: the future energy carrier". In: *Philosophical Transactions of the Rocyal Society* 368.1923 (2010). DOI: 10.1098/rsta.2010.0113.

[2] T. Hübert et al. "Hydrogen sensors – A review". In: *Sensors and Actuators B: Chemical* 157.2 (2011), pp. 329–352. DOI: 10.1016/j.snb.2011.04.070.

[3] Christoph Langhammer et al. "Hydrogen Storage in Pd Nanodisks Characterized with a Novel Nanoplasmonic Sensing Scheme". In: *Nano Letters* 7.10 (2007), pp. 3122–3127. DOI: 10.1021/nl071664a.

[4] Carl Wadell, Svetlana Syrenova, and Christoph Langhammer. "Plasmonic Hydrogen Sensing with Nanostructured Metal Hydrides". In: *Nano Letters* 8.12 (2014), pp. 11925–11940. DOI: 10.1021/nn505804f.

[5] Iwan Darmadi et al. "Rationally Designed PdAuCu Ternary Alloy Nanoparticles for Intrinsically Deactivation-Resistant Ultrafast Plasmonic Hydrogen Sensing". In: *ACS Sensors* 4.5 (2019), pp. 1424–1432. DOI: 10.1021/acssensors.9b00610.

[6] Rakesh Kumar et al. "Fast response and recovery of hydrogen sensing in Pd–Pt nanoparticle–graphene composite layers". In: *Nanotechnology* 22 (2011), pp. 275719–275726. DOI: 10.1088/0957-4484/22/27/275719.

[7] R. C. Hughes and W. K. Schubert. "Thin films of Pd/Ni alloys for detection of high hydrogen concentrations". In: *Journal of Applied Physics* 71.542 (1992). DOI: 10.1063/1.350646.

[8] Bharat Sharma and Jung-Sik Kim. "Pd/Ag alloy as an application for hydrogen sensing". In: *International Journal of Hydrogen Energy* 42.40 (2017), pp. 25446–25452. DOI: 10.1016/j.ijhydene.2017.08.142.

[9] K Yoshimura et al. "A hydrogen sensor based on Mg–Pd alloy thin film". In: *Measurement Science and Technology* 18.11 (2007), p. 3335. DOI: 10.1088/0957-0233/18/11/011.

[10] Martin Dornheim. *Thermodynamics of Metal Hydrides: Tailoring Reaction Enthalpies of Hydrogen Storage Materials*. 2011. DOI: 10.5772/21662.

[11] Brian D. Adams and Aicheng Chen. "The role of palladium in a hydrogen economy". In: *Materials Today* 14.6 (2011), pp. 282–289. DOI: 10.1016/S1369-7021(11)70143-2.

[12] Yuh Fukai. *The Metal-Hydrogen System, Basic Bulk Properties*. Springer-Verlag, Berlin, 2005, pp. 9–53.

[13] Kathryn M. Mayer and Jason H. Hafner. "Localized Surface Plasmon Resonance Sensors". In: *Chemical Reviews* 111 (2011), pp. 3828–3858. DOI: 10.1021/cr100313v.

[14] Christoph Langhammer et al. “Plasmonic Properties of Supported Pt and Pd Nanostructures”. In: *Nano Letters* 6.4 (2006), pp. 833–838. DOI: 10.1021/nl060219x.

[15] Urcan Guler and Rasit Turan. “Effect of particle properties and light polarization on the plasmonic resonances in metallic nanoparticles”. In: *Optics Express* 18.16 (2010), pp. 17322–17338. DOI: 10.1364/OE.18.017322.

[16] Christoph Langhammer et al. “Hydrogen Storage in Pd Nanodisks Characterized with a Novel Nanoplasmonic Sensing Scheme”. In: *Nano Letters* 7.10 (2007), pp. 3122–3127. DOI: 10.1021/nl071664a.

[17] Nikolai Strohfeldt, Andreas Tittl, and Harald Giessen. “Long-term stability of capped and buffered palladium-nickel thin films and nanostructures for plasmonic hydrogen sensing applications”. In: *Optical Materials Express* 2.3 (2013), pp. 194–204. DOI: 10.1364/OME.3.000194.

[18] Carl Wadell et al. “Hysteresis-Free Nanoplasmonic Pd–Au Alloy Hydrogen Sensors”. In: *Nano Letters* 15.5 (2015), pp. 3563–3570. DOI: 10.1021/acs.nanolett.5b01053.

[19] Ferry Anggoro Ardy Nugroho et al. “Universal Scaling and Design Rules of Hydrogen-Induced Optical Properties in Pd and Pd-Alloy Nanoparticles”. In: *ACS Nano* 12.10 (2018), pp. 9903–9912. DOI: 10.1021/acsnano.8b02835.

[20] David Monzón-Hernández et al. “Optical microfibers decorated with PdAu nanoparticles for fast hydrogen sensing”. In: *Sensors and Actuators B: Chemical* 151.1 (2010), pp. 219–222. DOI: 10.1016/j.snb.2010.09.018.

[21] E. G. Allison and G. C. Bond. “The Structure and Catalytic Properties of Palladium-Silver and Palladium-Gold Alloys”. In: *Catalysis Reviews* 7.2 (1972), pp. 233–289. DOI: 10.1080/01614947208062259.

[22] Z. Zhao et al. “All-optical hydrogen sensor based on a high alloycontent palladium thin film”. In: *Sensors and Actuators B* 113 (2006), pp. 532–538. DOI: 10.1016/j.snb.2005.03.070.

[23] E. G. Allison and G. C. Bond. “Achieving optimum hydrogen permeability in PdAg and PdAu alloys”. In: *Journal of Chemical Physics* 125.18 (2006). DOI: 10.1063/1.2387166.

[24] Mikhail Mamatkulov and Vladimir P. Zhdanov. “Suppression of hysteresis in absorption of hydrogen by a Pd-Au alloy”. In: *Physical Review E* 101.4 (2020), p. 042130. DOI: 10.1103/PhysRevE.101.042130.

[25] P.R. Subramanlan and D.E. Laughlin. “Cu-Pd (Copper-Palladium)”. In: *Journal of Phase Equilibria* 12 (1991), pp. 231–243.

[26] R. Burch and R. G. Buss. “Absorption of Hydrogen by Palladium-Copper Alloys”. In: *Journal of the Chemical Society* 71 (1975), pp. 913–921. DOI: 10.1039/F19757100913.

[27] Casey P. O’Brien and Ivan C. Lee. “The interaction of CO with PdCu hydrogen separation membranes: An operando infrared spectroscopy study”. In: *Catalysis today* 336 (2019), pp. 216–222. DOI: 10.1016/j.cattod.2017.09.039.

[28] Natalie Pomerantz and Yi Hua Ma. “Effect of H_2S on the Performance and Long-Term Stability of Pd/Cu Membranes”. In: *Industrial & Engineering Chemistry Research* 48.8 (2009), pp. 4030–4039. DOI: 10.1021/ie801947a.

[29] R. C. Hughes, W. K. Schubert, and R. J. Buss. "Solid-State Hydrogen Sensors Using Palladium-Nickel Alloys: Effect of Alloy Composition on Sensor Response". In: *Journal of the Electrochemical Society* 142.1 (1995), pp. 249–254.

[30] Ted B. Flanagan and H. Noh. "Thermodynamics and Hysteresis for Hydrogen Solution and Hydride Formation in Pd-Ni Alloys". In: *Zeitschrift für Naturforschung A* 50.4-5 (1995). DOI: 10.1515/zna-1995-4-522.

[31] Eunsongyi Lee et al. "Hydrogen gas sensing performance of Pd–Ni alloy thin films". In: *Thin Solid Films* 519.2 (2010), pp. 880–884. DOI: 10.1016/j.tsf.2010.07.122.

[32] A. Picciotto et al. "Evidence of plasmon resonances of nickel particles deposited by pulsed laser ablation". In: *Radiat Eff Defect Solid* 163 (2008), pp. 513–518. DOI: 10.1080/10420150701780656.

[33] I. Karakaya and Thompson W.T. "The Ag-Pd (Silver-Palladium) System". In: *Bulletin of Alloy Phase Diagrams* 9.3 (1988), pp. 237–243.

[34] H. Ziichner and T. Rauf. "Electrochemical isotherm measurements on the Pd-H and PdAg-H systems". In: *Journal of the Less-Common Metals* 17.174 (1991), pp. 816–823. DOI: 10.1016/0022-5088(91)90208-L.

[35] Chandrashekhar G. Sonwane, Jennifer Wilcox, and Yi Hua Ma. "Achieving optimum hydrogen permeability in PdAg and PdAu alloys". In: *Journal of Chemical Physics* 125.18 (2006), p. 184714. DOI: 10.1063/1.2387166.

[36] A. W. Carson and F. A. Lewis. "Pressure-composition Isotherms for the Pd+Ag+H System". In: *Transactions of the Faraday Society* 63 (1967), pp. 1453–1457. DOI: 10.1039/TF9676301453.

[37] Y. Sakamoto et al. "Thermodynamics of hydrogen absorption by Pd-Sb and Pd-Bi alloys". In: *International Journal of Hydrogen Energy* 21.11–12 (1996), pp. 1009–1015. DOI: 10.1016/S0360-3199(96)00064-X.

[38] Lingling Du et al. "Palladium/Bismuth Nanowires with Rough Surface for Stable Hydrogen Sensing at Low Temperatures". In: *ACS Applied Nano Materials* 2.3 (2019), pp. 1178–1184. DOI: 10.1021/acsanm.8b02029.

[39] Xiaofeng Chang et al. "Probing the light harvesting and charge rectification of bismuth nanoparticles behind the promoted photoreactivity onto Bi/BiOCl catalyst by (in-situ) electron microscopy". In: *Applied Catalysis B: Environmental* 201 (2017), pp. 495–502. DOI: 10.1016/j.apcatb.2016.08.049.

[40] A. K. M. Fazle Kibria and Y.Sakamoto. "The effect of alloying of palladium with silver and rhodium on the hydrogen solubility, miscibility gap and hysteresis". In: *International Journal of Hydrogen Energy* 25.9 (2000), pp. 853–859. DOI: 10.1016/S0360-3199(00)00006-9.

[41] Iwan Darmadi. "Polymer-Nanoparticle Hybrid Materials for Plasmonic Hydrogen Detection". PhD thesis. Chalmers University of Technology, 2021.

[42] Lei Shao and Jiapeng Zheng. "Fabrication of plasmonic nanostructures by hole-mask colloidal lithography: Recent development". In: *Applied Materials Today* 15 (2019), pp. 6–17. DOI: 10.1016/j.apmt.2018.12.014.

[43] Brian D. Adams, Cassandra K. Ostrom, and Aicheng Chen. "Hydrogen Electrosorption into PdCd Nanostructures". In: *Langmuir* 26.10 (2010), pp. 7632–7637. DOI: 10.1021/la9044072.

[44] Gerhard L. Holleck. “Diffusion and Solubility of Hydrogen in Palladium and Palladium-Silver Alloys”. In: *Journal of Physical Chemistry* 74.3 (1970), pp. 503–511. DOI: 10.1021/j100698a005.

DEPARTMENT OF SOME SUBJECT OR TECHNOLOGY
CHALMERS UNIVERSITY OF TECHNOLOGY
Gothenburg, Sweden
www.chalmers.se

CHALMERS
UNIVERSITY OF TECHNOLOGY